# Aircraft to aircraft intercomparison during SEMAPHORE

Dominique Lambert, Pierre Durand

JOURNAL OF GEOPHYSICAL RESEARCH, VOL. 103, NO. C11, PAGES 25,109-25,123, OCTOBER 15, 1998

# Aircraft to aircraft intercomparison during SEMAPHORE

Dominique Lambert and Pierre Durand[1]

Laboratoire d'Aérologie, Unité Mixte de Recherche CNRS/Université Paul Sabatier 5560, Observatoire Midi-Pyrénées, Toulouse, France

**Abstract.** During the Structure des Echanges Mer-Atmosphère, Propriétés des Hétérogénéités Océaniques: Recherche Expérimentale (SEMAPHORE) experiment, performed in the Azores region in 1993, two French research aircraft were simultaneously used for in situ measurements in the atmospheric boundary layer. We present the results obtained from one intercomparison flight between the two aircraft. The mean parameters generally agree well, although the temperature has to be slightly shifted in order to be in agreement for the two aircraft. A detailed comparison of the turbulence parameters revealed no bias. The agreement is good for variances and is satisfactory for fluxes and skewness. A thorough study of the errors involved in flux computation revealed that the greatest accuracy is obtained for latent heat flux. Errors in sensible heat flux are considerably greater, and the worst results are obtained for momentum flux. The latter parameter, however, is more accurate than expected from previous parameterizations.

## 1. Introduction

An aircraft is an excellent platform for exploring the atmospheric boundary layer (ABL). This is why aircraft are frequently employed in cooperative field experiments. Aircraft can be used for both in situ and remote measurements. In the first case, several platforms often perform common measurements (like thermodynamics) in coordinated missions. The accuracy of each sensor has therefore to be analyzed in order to incorporate all the measurements in the analysis. Absolute calibration of most instruments is difficult because the measurements are affected by the airspeed of the sensor. Calibration against ground-based measurements cannot be considered as satisfactory because the sampled areas and the sampling time are different for the two platforms. Furthermore, ground-based measurements generally cannot be used over the open ocean.

To provide accurate measurement from an aircraft requires (1) calibration of the sensor in the laboratory, (2) knowledge of the airflow around the sensor mounted on the aircraft in order to take into account the pressure contamination, and (3) determination of the final calibration from in-flight maneuvers [*Lenschow*, 1986]. Taking into account that there is no absolute reference for in-flight measurements, aircraft-to-aircraft intercomparisons are often the best way to ensure coherence between the various platforms. Such experiments were already performed by *Nicholls et al.* [1983], *Lenschow et al.* [1991], *Strom et al.* [1994], *Quante et al.* [1996], *Dobosy et al.* [1997], and *Lucotte and Saïd* [1996]. Comparisons generally concern the mean parameters like temperature, moisture, wind, and scalars and the turbulence moments like variance and flux for these parameters. They could also include radiation measurements. Furthermore, a comparison of turbulence scales measured by a dual aircraft formation has already been performed by *Lenschow and Kristensen* [1988].

This paper examines an intercomparison flight of two French atmospheric research aircraft used in the Structure des Echanges Mer-Atmosphère, Propriétés des Hétérogénéités Océaniques: Recherche Expérimentale (SEMAPHORE) experiment. After a presentation of the campaign and of the instrumentation for the two aircraft, we introduce the intercomparison flight in section 3. Section 4 is a presentation of the intercomparison results for both mean parameters and second-order turbulence moments. In section 5, we analyze the errors involved in computation of the turbulent flux; we present a direct estimation of these errors deduced from measurements of the two aircraft, which is compared to parameterizations found in the literature.

## 2. Presentation of the Campaign and of the Aircraft Instrumentation

### 2.1. The Campaign

The SEMAPHORE experiment [*Eymard et al.*, 1996] was conducted in the Azores region in fall 1993 and focused on studies of oceanic and atmospheric mesoscale circulations, as well as on interactions between the oceanic and atmospheric boundary layers. From October 4 to November 17, two instrumented aircraft (the Merlin IV from the French Meteorological Office Météo-France and the Fokker 27 (hereafter called ARAT, french acronym for atmospheric and remote sensing research aircraft) instrumented by the Institut National des Sciences de l'Univers) were frequently employed for coordinated missions. During this period, the aircraft were used with a succession of various in situ and remote sensing instruments. This paper only deals with in situ thermodynamics and turbulence measurements, which were performed during 54 flights. Among them, 40 flights corresponded to 20 experiments during which the two aircraft

[1]Now at Centre National de Recherches Météorologiques / Groupe de Météorologie Expérimentale et Instrumentale, Météo-France, Toulouse, France.



Paper number 97JC02199.
0148-0227/98/97JC-02199$09.00

flew in the ABL at the same period and over the same area. To use the set of SEMAPHORE aircraft data therefore requires a thorough intercomparison between the two aircraft. Owing to frequently coordinated aircraft and ship measurements, *Durand et al.* [this issue] performed a comparison between surface flux measured onboard the R/V *Le Suroît* and extrapolated toward the surface from airborne measurements performed in the ABL.

### 2.2. Aircraft Instrumentation and Data Processing

In this section, we will describe the aircraft instrumentation for in situ measurements. The main sensors on board the aircraft are designed in order to measure the three wind components, the temperature, and the air moisture for both the mean values and the fluctuation (except for the mean vertical velocity which cannot be accurately measured). The main sensors, routinely used, are listed in Table 1. For most of the parameters, one or several "spare" measurement systems are installed, but they are not indicated in Table 1. For example, three temperature probes are present on each aircraft (see section 4.2). Additional measurements, presented in Table 1, concern radiation.

The temperature is measured by a platinum wire, 30 μm in diameter, sheltered in a housing, and shaped to ensure that airflow velocity with respect to the wire is near zero. The measured value is therefore close to the total temperature. A correction of the adiabatic heating of the air (compressed to the total pressure) is then applied in order to deduce the air static temperature.

The specific humidity is computed from the measurement of the dew point temperature by a cooled-mirror, dew point hygrometer. This sensor provides an absolute measurement without drift with time, but it has a time response of from one to several seconds, and it cannot therefore be used for turbulence measurements. Fast response measurements are performed with a Lyman-α sensor (which measures the light absorption at 121.56 nm). The latter is calibrated against the specific humidity deduced from the dew point measurement. The Lyman-α sensor, in fact, measures the vapor density (expressed, for example, in g $m^{-3}$), and latent heat flux computation therefore requires correction to take into account the fluctuations in air density (the so-called "Webb correction" [*Webb et al.*, 1980]). Given the low values of sensible heat flux during SEMAPHORE, this correction is negligible.

The most complex measurements concern the three wind components. The wind vector is computed as the sum of the ground speed (GS) and true-airspeed (TAS) vectors. The result is, in general, an order of magnitude smaller than each of these two terms and so requires careful measurements and calibrations. The three components of the GS vector are measured by the inertial navigation system (INS). The same INS is installed aboard the two aircraft. It contains a mechanized platform. The INS has its own computer which performs real-time coupling (between barometric and accelerometric measurements) based on a Kalman filtering method. The three components of the TAS vector are computed from the module $V$ and the two angles of attack (α) and sideslip (β). $V$ is computed from the dynamic pressure $\Delta P$ (difference between the total and static pressure). Here α and β are computed from the differential pressure ($\delta P_\alpha$ and $\delta P_\beta$, respectively) measured on half a sphere between two points located on a vertical and a horizontal meridian, respectively. For the angle of attack, for example, we have

$$\alpha = \frac{\delta P_\alpha}{k_\alpha \Delta P}$$

where $k_\alpha$ is a constant depending on the angle between the two pressure ports. A similar relation is used for the sideslip angle. A central hole on the hemisphere is used as a port for the total pressure. On the Fokker 27, such a hemisphere (2 cm in diameter) is formed by the front of the Rosemount 858 probe, installed at the tip of a 6 m long nose boom, on which are also installed the temperature and Lyman-α probes. On the Merlin IV, the hemisphere is the nose of the aircraft, following the "radome" principle described by *Brown et al.* [1983]. A picture of these two systems (nose boom and radome) can be found in work by *Druilhet and Durand* [1997]. The static pressure ports are located on the cylindrical portion of the Rosemount 858 for the Fokker 27 and on the fuselage for the Merlin IV. The static defect, computed from specific maneuvers (low-altitude runs over the landing track), is taken into account in the values of the static and dynamic pressure. The three wind components ($u_E$, $u_N$, and $w$ in the east, north, and vertical direction, respectively) are then computed according to the simplified formulae (assuming small angles, except for the aircraft heading) of *Lenschow* [1986]

$$u_N = U_N - M\cos(\Psi+\beta) - l\dot{\Psi}\sin\Psi \quad (1)$$

$$u_E = U_E - M\sin(\Psi+\beta) + l\dot{\Psi}\cos\Psi \quad (2)$$

$$w = W + M(\alpha-\Theta) + l\dot{\Theta} \quad (3)$$

where Ψ and Θ are the true heading and the pitch angle of the aircraft (measured by the INS), respectively; $U_E$, $U_N$, and $W$ are the three components of the GS in the (east, north, vertical) coordinate system; and $l$ is the distance between the INS and the anemometric measurements; it is considerable for the Fokker 27 ($l \approx 11$ m), whereas on the Merlin IV the INS is installed close to the nose of the aircraft, and the terms including $l$ in the above equations can be neglected. These equations are used to calculate the instantaneous wind. On a given aircraft run (for example, 30 km of straight and constant level flight) the turbulent fluctuations are defined with respect to the average components on this run. The average vertical wind is set to zero because the values in the boundary layer (in the order of, say, $10^{-2}$ m $s^{-1}$) are lower than the expected accuracy for this component.

Radiation measurements involve upward and downward, shortwave and longwave radiation. The sum of these four terms therefore represents the net radiation at the aircraft flight level. The sea surface radiometric temperature is measured by a Barnes Precision Radiation Thermometer 5 on board each aircraft. Calculation of the sea surface temperature from this kind of measurement therefore requires knowledge of the surface emissivity. Furthermore, if the emissivity significantly differs from unity, a correction depending on the incoming longwave radiation has to be made. This correction can differ by as much as 0.4°C between an area without cloud and an area covered by low-altitude cloud, like stratocumulus. In the end, the absorption by the atmospheric layer between the surface and the flight level has to be corrected. This term is around 0.002 K $m^{-1}$.

**Table 1.** Main Instrumentation of the Two Aircraft

| Measured parameter | Fokker 27 Sensor | Merlin IV Sensor | Range of Measurement | Fokker 27 Sampling Rate, $s^{-1}$ | Merlin IV Sampling Rate, $s^{-1}$ |
|---|---|---|---|---|---|
| | | *Thermodynamics* | | | |
| temperature | Rosemount 102E2AL | Rosemount 102E2AL | ±50°C | 64 | 25 |
| static pressure | Rosemount 858 on the nose boom and transducer Crouzet 43 | static ports on fuselage and transducer Rosemount 1201 | 0-1050 hPa | 16 | 25 |
| specific humidity | Lyman α AIR-LA1 | Lyman α AIR LA1 | 0 - 20 g $m^{-3}$ | 256 | 25 |
| dew point temperature | General Eastern 1011B | General Eastern 1011B | -75°-50°C | 8 | 25 |
| liquid water content | Johnson Williams CT7 | Johnson William CT43 | 0-6 g $m^{-3}$ | 16 | 1 |
| | | *Dynamics* | | | |
| dynamic pressure | Rosemount 858 on the nose boom and transducer Crouzet 44 | total pressure port on radome and static pressure port on fuselage and transducer Rosemount 1221F | 0-100 hPa | 64 | 25 |
| attack angle (α) and sideslip angle (β) | pressure ports on Rosemount 858 and 2 transducers Rosemount 1221F | pressure ports on Radome and 2 transducers Rosemount 1221F | ±35 hPa | 64 | 25 |
| true heading | INS* Sagem ULIS 45 I | INS* Sagem ULIS 45 I | 0 - 360° | 64 | 25 |
| roll | id. | id. | ±180° | 64 | 25 |
| pitch | id. | id. | ±180° | 64 | 25 |
| longitude | id. | id. | ±180° | 4 | 5 |
| latitude | id. | id. | ±90° | 4 | 5 |
| groundspeed (north, east, and vertical) | id. | id. | ±1075m/s (horitontal) and ±45m/s (vertical) | 64 | 25 |
| altitude above the surface | Radioaltimeter TRT AHV12 | Radioaltimeter TRT ERT900 | 0 - 5000 m | 16 | 25 |
| | | *Radiation* | | | |
| upward and downward, shortwave radiation (2π St.) | 2 pyranometers Eppley PSP (0.2-2.7 μm) | 2 pyranometers Eppley PSP (0.2-2.7 μm) | 0-1500 W $m^{-2}$ | 4 | 1 |
| upward and downward, longwave radiation (2π St.) | 2 pyrgeometers Eppley PIR (4-40 μm) | 2 pyrgeometers Eppley PIR (4-40 μm) | 0-600 W $m^{-2}$ | 4 | 1 |
| surface radiometric temperature | downward looking, PRT5 Barnes radiometer (8-14 μm) | downward looking, PRT5 Barnes radiometer (8-14 μm) | -20°-75°C | 16 | 1 |
| sky radiometric temperature | upward looking, PRT5 Barnes radiometer (8-14 μm) | | -80°-15°C | 16 | |

The "spare" sensors are not indicated. Note that the measurement range of the attack and sideslip angle is given in hPa because the measured parameters are differential pressures (see text for more explanations). * INS: Inertial Navigation System.

The sampling rate of the various parameters varies according to the time response of the sensors (see Table 1). The parameters involved in turbulence calculation are acquired at a rate of 64 $s^{-1}$ on the Fokker 27 (except for the Lyman-$\alpha$ signal, acquired at 256 $s^{-1}$) and 25 $s^{-1}$ on the Merlin IV. The turbulence moments were computed on the time series defined at 16 $s^{-1}$ for the Fokker 27 (after averaging) and 25 $s^{-1}$ for the Merlin. These rates are sufficient to encompass those scales which significantly contribute to turbulent energy in the boundary layer [see *Durand et al.*, this issue].

The aircraft's geographical horizontal position is determined by the INS. The altitude of the aircraft is determined either by means of the static pressure (which requires knowledge of the surface pressure) or by the radio altimeter, which measures the altitude above the overflown surface and whose expected accuracy is around 2%. For measurements in the boundary layer over the sea, the latter system is preferred.

## 3. The Intercomparison Flight

This intercomparison flight was conducted on November, 5, 1993, between 1120 and 1250 UT. During this flight the two aircraft were equipped for in situ measurements. The meteorological conditions were those frequently encountered during the SEMAPHORE experiment; a moderate wind blew from north to northeast (about 8 m $s^{-1}$ in the ABL), and the ABL was topped by a broken stratocumulus layer extending from 1500 to 1800 m and capped by a sharp temperature inversion together with important drying.

The flight area was centered 50 km to the east of the island of Santa Maria, i.e., given the wind direction, outside of the archipelago wake. The flight track (Figure 1) consisted of a horizontal square with about 30 km sides performed at 90 m above the surface. This was followed by four horizontal runs, 25 to 30 km long and at 300 m altitude, the first two parallel to the mean wind and the last two with reverse headings perpendicular to the mean wind. This flight pattern was chosen in order to improve calculation of the mean wind. Finally, a slant ascent between 30 and 2400 m was realized in the same area.

In most papers dealing with aircraft-to-aircraft intercomparison the platforms fly in close formation ("wing-to-wing") with a quasi-constant horizontal distance between them. One advantage of this maneuver is that the aircraft analyze the same air parcels, at least for scales greater than the distance between the platforms [*Lenschow and Kristensen*, 1988]. Another advantage is that most of the measured parameters can be compared, including TAS, groundspeed, and horizontal and vertical position of the aircraft. However, this maneuver constrains the aircraft to fly at a common airspeed, which is sometimes different from their usual measurement airspeed.

In the experiment analyzed here, each aircraft flies at its own usual airspeed, which is slightly greater for the Merlin IV than for the Fokker 27. Consequently, the distance between the two aircraft can reach 4 min in time and 25 km in a horizontal direction. We will assume stationarity for a straight and level run analyzed by the two aircraft and compare the quantities averaged along the runs (mean temperature, moisture, and wind and turbulence moments). On this particular day, wind in the boundary layer was about 8 m $s^{-1}$. Consequently, for a time delay of 4 min between the two aircraft (which constitutes the maximum delay), the airmass

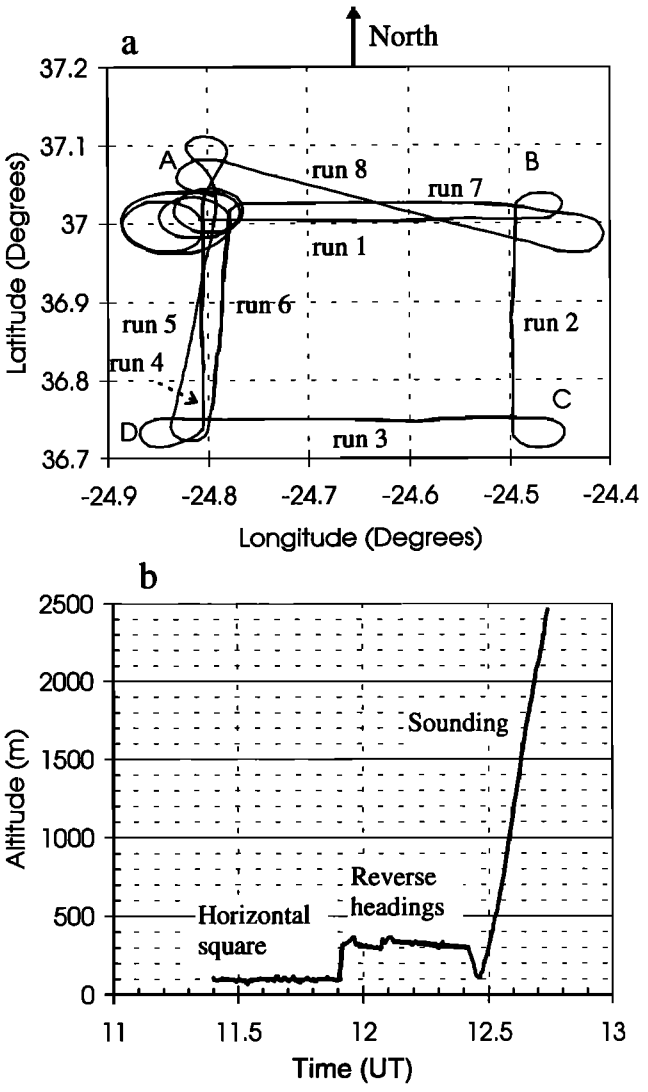


**Figure 1.** (a) Ground track and (b) profile of the intercomparison flight. The eight straight and level runs are indicated on Figure 1a.

was displaced by about 1.9 km. This distance is 1 order of magnitude lower than the length of the runs (about 25 to 30 km). On along-wind runs the two aircraft are in the same air mass for most of the run, whereas for cross-wind runs they fly in different air parcels. To compute the turbulence moment, we must assume horizontal homogeneity at the scale of the runs, i.e., 25 to 30 km. We can therefore consider that similar samples are analyzed by the aircraft for both along-wind and cross-wind runs. However, the horizontal distance between the aircraft being at least 1 order of magnitude greater than the turbulence characteristic scales, we will consider that the estimations of a turbulent moment along a run by the two aircraft constitute two independent realizations of this moment. This will be used later.

## 4. Intercomparison Results

### 4.1. Aircraft Position

We define the horizontal aircraft position from the INS. During SEMAPHORE we did not test the accuracy of this instrument, but we noted that the error at the end of each

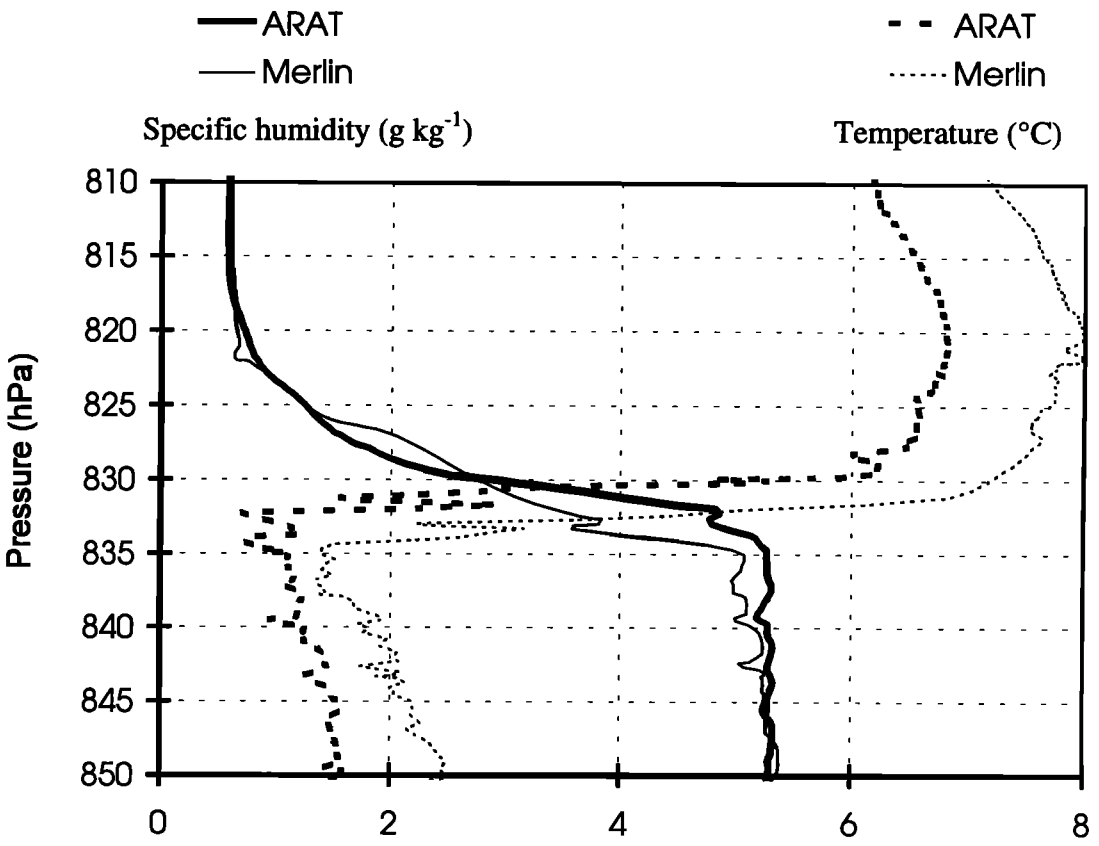


**Figure 2.** Profile of the specific humidity and of the potential temperature measured by the two aircraft in a 40 hPa thickness layer around the inversion level.

flight was in the expected range; that is, the time drift in the horizontal position was within 1 km $h^{-1}$.

We can obtain the vertical position from two sensors: first, the static pressure whose expected accuracy is about 2 hPa, which leads to an altitude accuracy of about 20 m if we know the sea level pressure and second, the radioaltimeter whose expected accuracy is about 2% and which works in the 0-5000 m range. Sounding was used to control the quality of the pressure coordinate: in the SEMAPHORE measurement area, there is still a capping inversion of temperature at the top of the stratocumulus layer. With this inversion, there is still a strong fall in humidity. We can see on Figure 2 that the inversion is seen by the two aircraft with a pressure difference of about 2 hPa. This difference is within the expected error range. So we can use the pressure coordinate as a reference for altitude, provided that the sea surface pressure is known. This coordinate can be used when its accuracy becomes better than that of the radio altimeter altitude, i.e., above 1000 m.

### 4.2. Thermodynamics

**4.2.1. Temperature.** There are three temperature sensors aboard each aircraft: a platinum wire in a Rosemount antenna, another similar sensor but with deicing, and a "reverse flow" probe for in-cloud measurements. Without icing conditions and out of clouds the first sensor is usually used for mean and turbulence measurements. The latter two are not sufficiently fast for turbulence measurements.

Figure 3 shows the temperature profiles measured by these six sensors in a layer of 50 hPa thickness. The difference can reach 1 K. The three Fokker measurements are lower than the Merlin ones. The Fokker measured temperatures are on average 0.5 K lower than those of the Merlin. However, three of the six sensors give close values (within 0.15 K): the Fokker Reverse Flow, the Merlin deiced Rosemount, and the Merlin Reverse Flow. So we choose as a reference the Merlin deiced Rosemount probe. We will therefore obtain better coherence between all the measurements in correcting the other sensors. Table 2 presents the results of the comparison performed on the mean and turbulent parameters averaged along each of the eight straight and level runs. The indicated values are, for a parameter $X$, the mean difference between the two aircraft $\Delta X$, the root-mean square (rms.) of the difference $\sigma_{\Delta x}$, and the ratio of $\sigma_{\Delta x}$ to the mean value between the two aircraft, $\sigma_{\Delta x}$ / $\langle X \rangle$ (provided that this parameter was not meaningless). With respect to the temperature computed from the Rosemount nondeiced probe, the difference reaches 1 K.

**4.2.2. Humidity.** We only present here comparisons between dew point hygrometers, two of them being installed on each aircraft. In Figure 4, we present the profile of the dew point temperature measured during the sounding. Because of the expected accuracy (0.5 K, that is to say about 0.2 g $kg^{-1}$ in the boundary layer) we cannot see any significative difference between the sensors. Above the inversion the measurements are less accurate, but water content is very low (0.5 g $kg^{-1}$ at 750 hPa).

**4.2.3. Horizontal wind measurements.** Figure 5 presents a comparison of the mean wind computed on the eight straight and level runs. There is no bias between the two aircraft, and

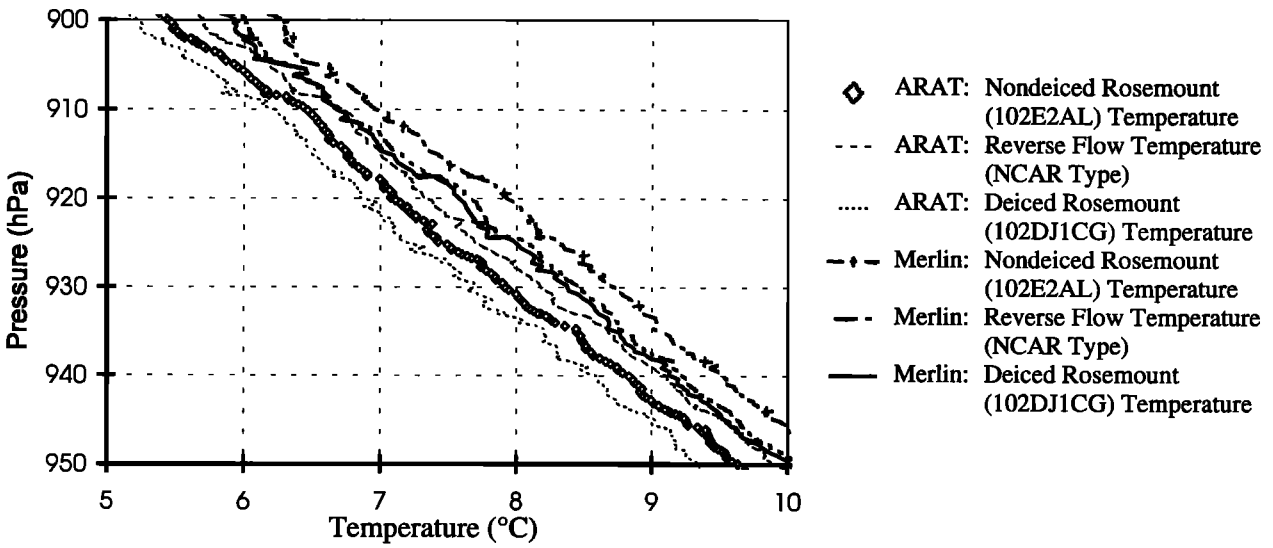


**Figure 3.** Comparison of the temperature profiles measured by the six sensors in a layer of 50 hPa thickness.

dispersion is about 0.5 m $s^{-1}$ and 3.5°, which is satisfactory. We must, however, keep in mind that error in the wind calculation from an aircraft is not a random error. In general, this error is almost constant on a flight axis stabilized in heading and altitude. This error varies according to the aircraft heading. So, if we consider two axes with reverse headings, for example, the difference between the wind calculations on these two axes will be equal to twice the error on each axis. For this reason it is very difficult to obtain an estimation of the wind vertical gradients from superposed axes with reverse

**Table 2.** Results of the Comparison Performed on the Mean and Turbulent Parameters Averaged Along Each of the Height Straight and Level Runs

| | $\Delta$ | $\sigma_\Delta$ | $\sigma_\Delta/\langle x\rangle$ |
|---|---|---|---|
| $T$, °C | -1.10 | 0.14 | |
| $q$, g $kg^{-1}$ | 0.12 | 0.15 | |
| Wind speed, m $s^{-1}$ | -0.02 | 0.54 | 0.07 |
| Wind direction, deg. | -0.20 | 3.5 | |
| Dissipation rate of TKE, $m^2$ $s^{-3}$ | 0.00004 | 0.00011 | 0.19 |
| $\lambda_{mi}$, m | 139 | 487 | 0.51 |
| $\sigma_\theta$, K | -0.0042 | 0.0032 | 0.07 |
| $\sigma_q$, g $kg^{-1}$ | 0.015 | 0.017 | 0.11 |
| $\sigma_u$, m $s^{-1}$ | -0.01 | 0.08 | 0.14 |
| $\sigma_v$, m $s^{-1}$ | 0.02 | 0.07 | 0.13 |
| $\sigma_w$, m $s^{-1}$ | 0.0047 | 0.05 | 0.08 |
| $H$, w $m^{-2}$ | -2.30 | 6.1 | 0.44 |
| $LE$, w $m^{-2}$ | 2.30 | 41.8 | 0.28 |
| $-\tau/\rho$, m $s^{-2}$ | 0.002 | 0.04 | 0.67 |
| $\overline{u'w'}$, m $s^{-2}$ | 0.002 | 0.036 | -0.75 |
| $\overline{v'w'}$, m $s^{-2}$ | -0.001 | 0.049 | -2.04 |
| $r_{\theta'q'}$ | -0.10 | 0.11 | 0.21 |
| $r_{w'q'}$ | -0.05 | 0.10 | 0.18 |
| $r_{w'\theta'}$ | -0.04 | 0.14 | 0.36 |
| TKE, m $s^{-2}$ | 0.01 | 0.07 | 0.13 |
| $\overline{w'\,\mathrm{TKE}}$, m $s^{-3}$ | 0.0002 | 0.078 | 0.76 |
| $S_\theta$ | -0.10 | 0.27 | 0.41 |
| $S_q$ | -0.06 | 0.28 | 0.29 |
| $S_u$ | 0.07 | 0.14 | -2.76 |
| $S_v$ | -0.09 | 0.37 | -4.59 |
| $S_w$ | 0.02 | 0.24 | 0.56 |

The indicated values are, for a parameter $X$, the mean difference between the two aircraft $\Delta X$ (difference Fokker-Merlin), the rms of this difference $\sigma_{\Delta x}$, and the ratio of $\sigma_\Delta$ to the mean value between the two aircraft, $\sigma_{\Delta x} / \langle X\rangle$ (provided that this parameter was not meaningless). Here $\sigma_\theta$, $\sigma_q$, $\sigma_u$, $\sigma_v$, and $\sigma_w$ are the standard deviation of the potential temperature, the specific humidity, the longitudinal, transversal, and vertical wind speed, respectively; H is the sensible heat flux, LE the latent heat flux, and $\tau$ is the total momentum flux; $\overline{u'w'}$ and $\overline{v'w'}$ are the longitudinal and transversal wind flux; $r_{x'y'}$ is the correlation coefficient; TKE is the turbulent kinetic energy; $\overline{w'\,\mathrm{TKE}}$ is the vertical flux of TKE; and $S_X$ is the skewness of $X$.

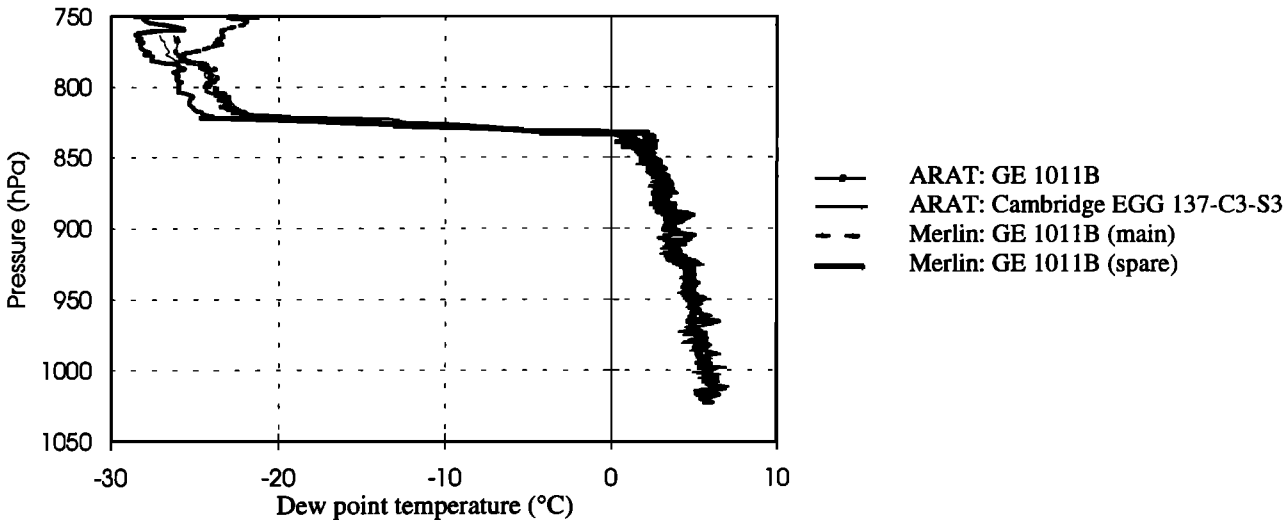


**Figure 4.** Dew point temperature profiles mesured by the two aircraft.

headings. This can explain the absence of bias between the aircraft when we use a closed track like here (four perpendicular axes).

### 4.3. Turbulence

Turbulence characteristics were computed on straight and level runs of 25 to 30 km long, which corresponds to 4 to 6 min flight time. This length is a compromise between the minimum distance required to properly describe the turbulence energy and the wish to reduce this distance in order to have access to the spatial variability of the turbulence moments. Furthermore, on the analyzed runs, the hypothesis of horizontal homogeneity must be valid.

The choice of the frequency range that will be used for the calculation is fundamental. For high frequencies this problem is easy to solve because the turbulent energy spectra decrease as a -5/3 power law according to frequency and the cospectra decrease as a -7/3 power law (Kolmogorov relations in the inertial subrange). For data processing, the raw parameters were reduced to a rate of 16 $s^{-1}$ for the Fokker 27 and 25 $s^{-1}$ for the Merlin IV, which corresponds to a spatial resolution of about 5 and 4 m, respectively. This is sufficient to capture most of the significant energy. The problem is more difficult for the lowest frequencies. The sample length (25 to 30 km) is a limit. Furthermore, a high-pass filtering of the signals is required before any turbulence moment calculation, in order to eliminate the lowest frequencies of the signals. All the SEMAPHORE calculations were made with a high-pass filtering cutoff of 0.01728 Hz for the Fokker and 0.01844 Hz for the Merlin. Given the aircraft airspeeds, these values correspond to about 5 km. We will justify the choice of this value later on. The numerical filtering is made on the Fourier transform. This operation does not therefore modify the phases of the signals. The consequences of this filtering on the flux values are discussed by *Durand et al.* [this issue].

The fluctuations of the three wind components, of the potential temperature, and of the specific humidity are thus calculated. The variances of these five parameters and their covariances taken two by two are calculated with the eddy-correlation technique. The horizontal wind components are computed in a coordinate system aligned with the mean wind of the run; the "*u*" component is aligned with the mean wind, whereas the "*v*" component is oriented 90° to the right of *u*. The sensible and latent heat fluxes and the momentum flux are deduced from the corresponding covariances. For the turbulence calculations the fluctuations used are the differences between the instantaneous and the mean value.

**4.3.1. Spectral characteristics.** From the energy spectrum of the vertical velocity, $S(n)$, where $n$ is the frequency, we can calculate two fundamental quantities: the dissipation rate of turbulent kinetic energy and a characteristic length scale, $\lambda_m$, defined as the wavelength of the maximum of $nS(n)$. The dissipation rate $\varepsilon$ is calculated in the high-frequency part of the spectrum with the Kolmogorov relation

$$S(k) = (4/3)\alpha\, \varepsilon^{2/3} k^{-5/3} \tag{4}$$

In this relation, the conversion of wave number ($k$) into frequency ($n$) is done with the hypothesis of frozen turbulence, $k = 2\pi n / TAS$. Here $\alpha$ is the Kolmogorov constant. The technique used to calculate $\lambda_m$ is also used to fit $nS(n)$ with an analytical relation like

$$nS(n) = \frac{a\,n}{1 + 1.5(n/n_m)^{5/3}} \tag{5}$$

where $a$ is a constant and $n_m$ = TAS/$\lambda_m$ is the frequency corresponding to the maximum of $nS(n)$.

The value of $\varepsilon$ was computed after filtering the vertical velocity signal in a band ($k_1$,$k_2$) where the wave numbers $k_1$ and $k_2$ lie in the inertial subrange. The variance of the filtered signal $\sigma_f^2$ can be related to $\varepsilon$ by integrating (4) between $k_1$ and $k_2$

$$\varepsilon = \sigma_f^{\,3}\left[2\alpha\left(k_1^{-2/3} - k_2^{-2/3}\right)\right]^{-3/2}$$

Similar techniques were already used by *Shaw and Businger* [1985] and *Druilhet et al.* [1985]. In Figure 6 we compare these spectral characteristics between the two aircraft. Here $\varepsilon$ presents good agreement between the two aircraft, with a very low bias and a scatter of 20% (see Table 2). The agreement between the length scales is excellent, except for one run on which the computed value from the Fokker 27 is more than twice that from the Merlin. The energy spectrum of this run

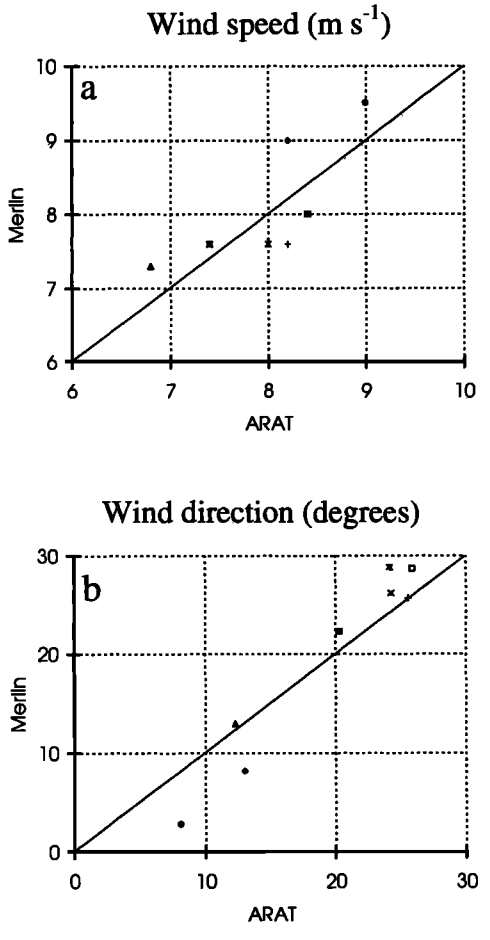


| Run | Symbol | Altitude (m) | Heading |
|---|---|---|---|
| 1 | ◆ | 96 | E |
| 2 | ● | 94 | S |
| 3 | ▲ | 94 | W |
| 4 | ■ | 95 | N |
| 5 | × | 297 | S |
| 6 | □ | 317 | N |
| 7 | + | 306 | E |
| 8 | ✱ | 296 | W |

**Figure 5.** Comparison of (a) the mean wind speed and (b) direction computed on the eight straight and level runs. The correspondence between the symbols and the runs of the pattern are indicated.

presents two maxima, probably related to the presence of coherent structures in the ABL. The analytical model (5), based on the existence of only one maximum of the energy spectrum, therefore fails in this case.

The cospectra represent how covariance is distributed in the frequency range described by the time series. Cospectra analysis is required in order to determine (1) whether the sampling rate is high enough to capture the smallest scales which contribute to the transfer, (2) whether the sample is long enough to capture the largest scales which contribute to the transfer, and (3) whether the high-pass filtering does not reduce the computed flux by a significant fraction. The two first criteria are satisfied if the cospectra vanish at the low- and high-frequency limits. Figure 7 presents the cospectra of vertical velocity and specific humidity (hereafter we will call them "latent heat flux cospectra"). The values represent the average of the four runs performed at the same altitude. The abscissa is the frequency divided by the average true airspeed of the aircraft (inverse of the wavelength). At $z$ = 90 m, the two first critera are well satisfied. A high-pass filtering at 1/5000 $m^{-1}$ does not significantly reduce the computed flux. At $z$ = 300 m, the cospectra are shifted toward lower frequencies. The length of the run is sufficient (the second criterion is satisfied), but the high-pass filtering probably reduces the computed flux. As will be explained below (see section 5), this filtering, however, is required to reduce the scatter of the results. Given the fluctuation of the cospectra, we do not exhibit any significant difference between the two aircraft. This fluctuation increases when the wavenumber decreases and is much more pronounced at 300 m than at 90 m. *Kaimal et al.* [1976] already noted that cospectra are very scattered above the atmospheric surface layer. It is therefore difficult to determine the cutoff frequency from the cospectra only. A thorough study of the errors resulting from high-pass filtering will be given in section 5.

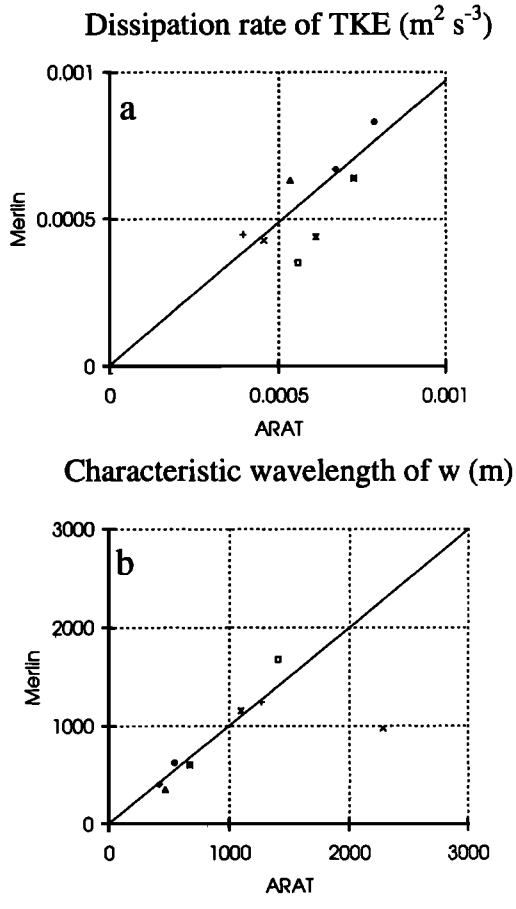


**Figure 6.** Comparison of the spectral characteristics. (a) Dissipation rate of turbulent kinetic energy (TKE) and (b) wavelength of the spectrum peak of the vertical velocity. See Figure 5 for the definition of the symbols.

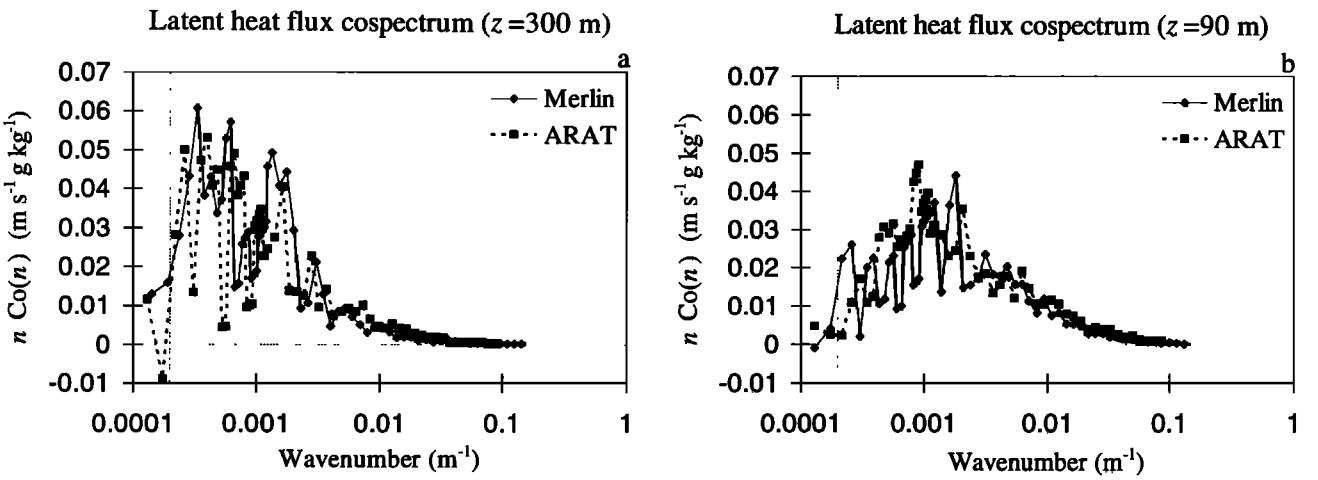


**Figure 7.** Average latent heat flux cospectra at (a) 300 m altitude and (b) 90 m altitude, for the Merlin IV and the Fokker 27. The vertical thin line indicates the wavelength of 5 km.

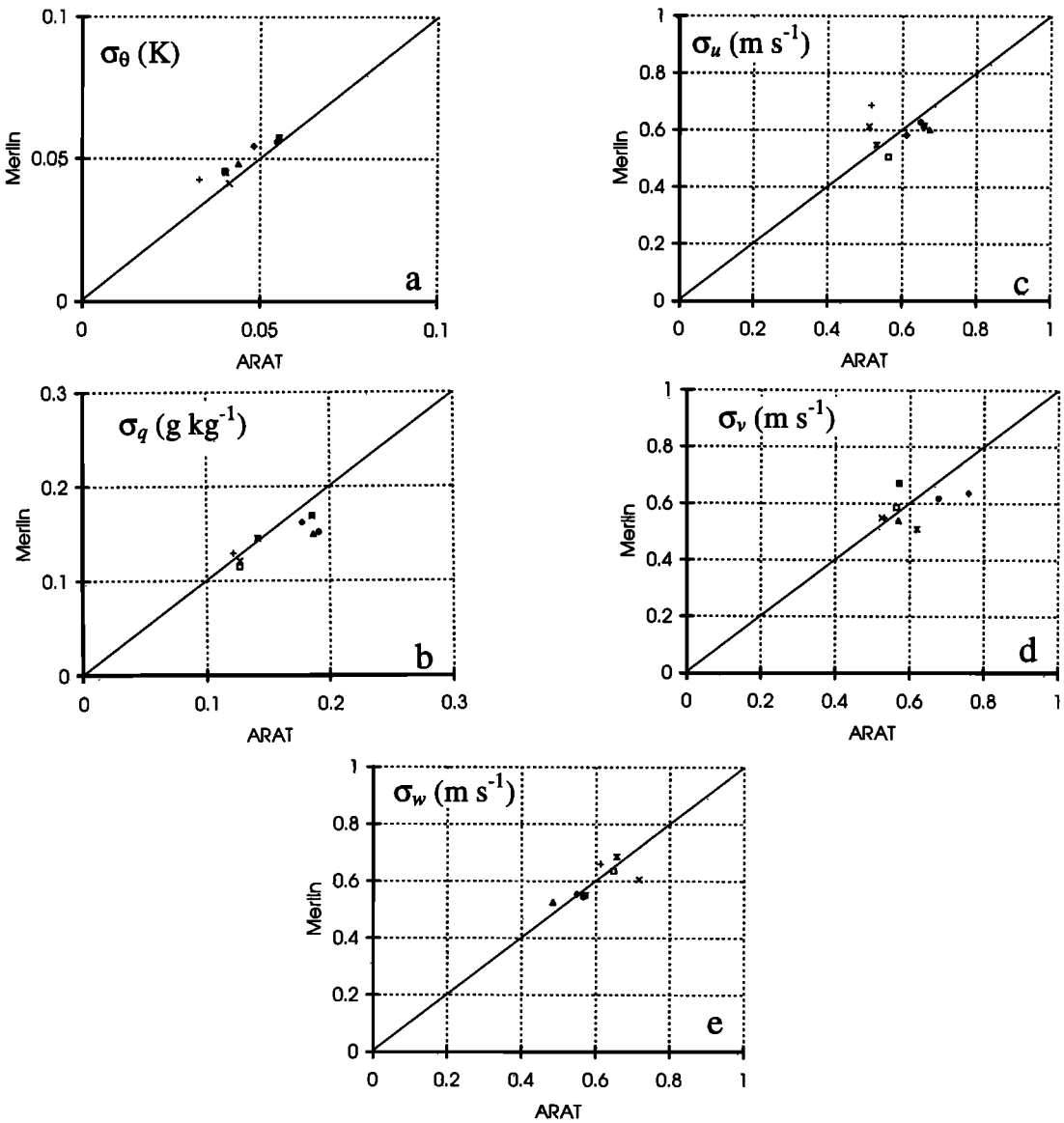


**Figure 8.** Comparison of the standard deviation of (a) potential temperature, (b) specific humidity, (c) longitudinal wind, (d) transversal wind, and (e) vertical wind. Signals were high-pass filtered with a cutoff wavelength of 5 km. See Figure 5 for the definition of the symbols.

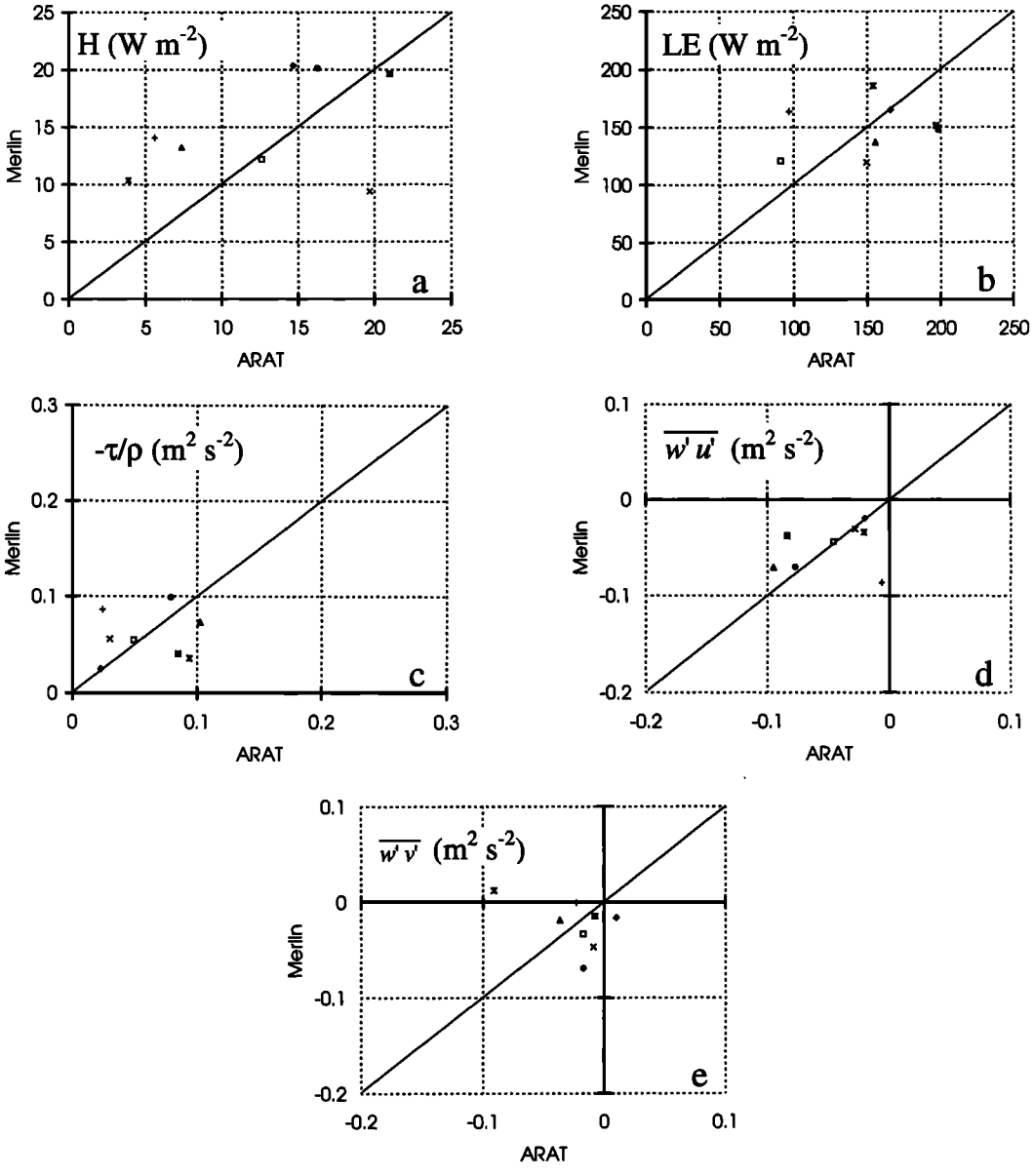


**Figure 9.** Comparison of (a) sensible heat flux, (b) latent heat flux, (c) total momentum flux (divided by the air density), (d) $\overline{w'u'}$, and (e) $\overline{w'v'}$ covariances. Signals were high-pass filtered with a cutoff wavelength of 5 km. See Figure 5 for the definition of the symbols.

**4.3.2. Turbulence moments.** In this section, we will compare moments obtained from high-pass filtered signals, with a cutoff wavelength of 5 km. Figure 8 shows the standard deviation of the five principal parameters. There is no important bias (see Table 2). Only the potential temperature shows slightly greater values for the Merlin, which can be explained by some noise in the upper part of the frequency spectrum (we shall discuss this point later). This bias is about 10% of the signal (that is to say about 20% for the variances). For all the presented parameters the scatter is about 10% of the mean value, which constitutes a satisfactory result.

Figure 9 shows fluxes and covariances. Latent and sensible heat flux values are representative of those encountered during the SEMAPHORE experiment: sensible heat flux is between 10 and 20 W $m^{-2}$ at low altitudes, and latent heat flux is about 150 W $m^{-2}$. For these two parameters, there is no bias between the two aircraft. The scatter is considerably greater for sensible heat flux (about 40% of the mean value) than for latent heat flux (about 25% of the mean value) (see Table 2). The low values of sensible heat flux probably explain this scatter.

The total momentum flux $\tau$ is calculated as the vectorial sum of the two components

$$-\tau / \rho = \left(\overline{u'w'}^2 + \overline{v'w'}^2\right)^{1/2}$$

where $\rho$ is the air density. We also present the covariances calculated along the two components; $u'$ is along the mean wind, and $v'$ is perpendicular. The result is not good. There is not much bias, but the scatter is as great as the mean value. We can probably explain this result as a problem of statistical

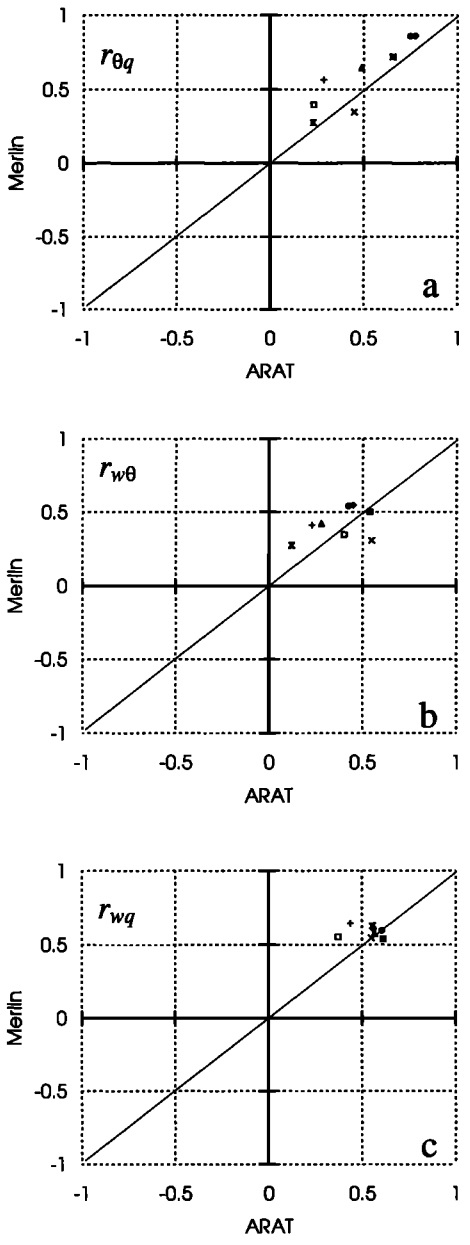


**Figure 10.** Comparison of correlation coefficients between (a) specific humidity and potential temperature, (b) vertical wind and potential temperature, and (c) vertical wind and specific humidity. Signals were high-pass filtered with a cutoff wavelength of 5 km. See Figure 5 for the definition of the symbols.

precision; the length scales for the momentum transfer are generally larger than those of the heat fluxes [*Lenschow and Stankov*, 1986]. Moreover, the total covariance is weak (about 0.05 $m^2$ $s^{-2}$ on average) and therefore more difficult to measure accurately. In fact, we can obtain this parameter with good accuracy near the surface in a zone with a vertical wind gradient, which allows satisfactory calculation of the friction velocity [see *Durand et al.*, this issue]. The wind speed was about 8 m $s^{-1}$ in the boundary layer, which is a value representative of the meteorological conditions of SEMAPHORE. So we should expect similar results for the other days, except for a few days with stronger wind.

From the covariances and standard deviations presented above we can calculate correlation coefficients. They are presented in Figure 10 for sensible heat flux, latent heat flux, and correlation between potential temperature and humidity. There is no major discrepancy. The scatter for sensible heat flux is a bit larger than for latent heat flux.

Figure 11 presents the turbulent kinetic energy (TKE) (per unit mass) and its vertical flux. The vertical gradient of this flux is one term of the TKE budget equation. For the intercomparison flight the TKE seems relatively constant, and the scatter is reasonable. The scatter is larger for the flux (about 100%) (see Table 2), but we have no bias between the two aircraft.

Figure 12 presents a comparison of the skewness of the five main parameters. The skewness of a parameter $X$ is defined as

$$S_x = \frac{\overline{x'^3}}{(\overline{x'^2})^{3/2}}$$

This parameter characterizes asymmetry in the distribution of the turbulent signals. So it is an indicator for the turbulence "organization." Skewness is a third-order moment, so we cannot expect as great an accuracy as for the variance. However, the scatter is about 0.24 to 0.28 for the temperature, the specific humidity, and the vertical velocity. However, horizontal wind components are more scattered, probably

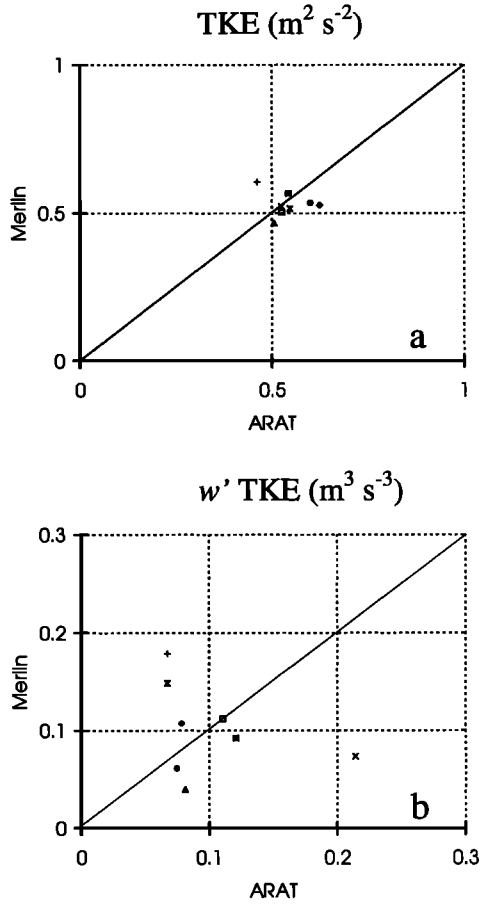


**Figure 11.** Comparison of (a) TKE (per unit mass) and (b) its vertical flux for high-pass filtered signals with a cutoff wavelength of 5 km. See Figure 5 for the definition of the symbols.

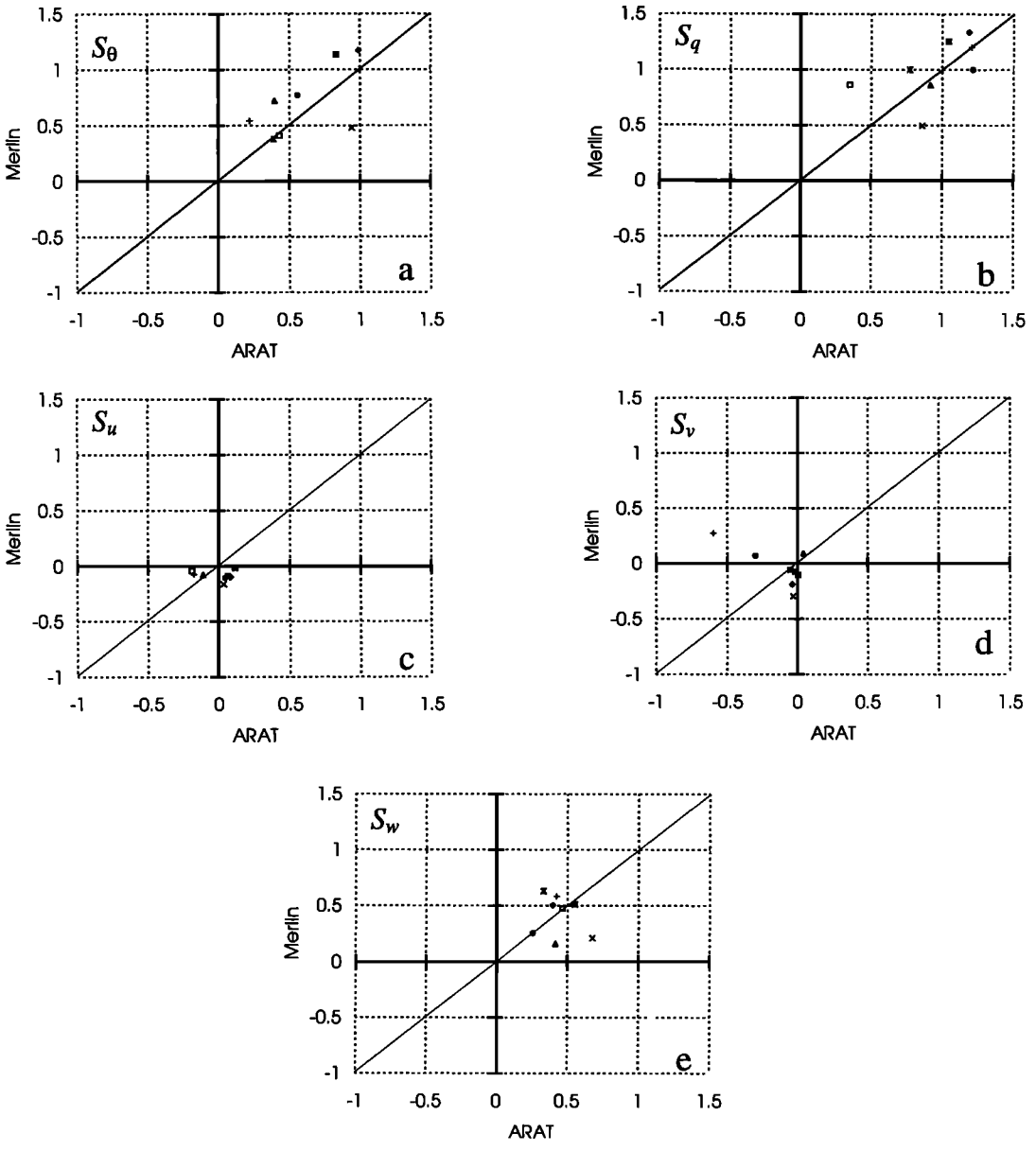


**Figure 12.** Comparison of the skewness of (a) potential temperature, (b) mixing ratio, (c) longitudinal wind, (d) transversal wind, and (e) vertical wind. Signals were high-pass filtered with a cutoff wavelength of 5 km. See Figure 5 for the definition of the symbols.

because of the importance of the low frequencies on these parameters.

## 5. Errors on the Turbulence Calculations

### 5.1. Definition

We do not here take instrument error into consideration. Turbulence moments are computed by the eddy-correlation method. The final error has two components: "systematic error" and "random error." For the variance and covariance calculations we eliminate part of the information with systematic high-pass filtering. This filtering can account for any systematic error. However, the analyzed sample is one realization of a random process; the characteristic scales of this process are described with limited precision, which is how random error is introduced. We must therefore analyze these characteristic scales in order to estimate the random error.

The systematic error $\varepsilon_s$ is defined as

$$\varepsilon_s = [F(L) - \langle F(L_c) \rangle] / F \tag{6}$$

where $F$ is the "true" value of the flux, $F(L)$ the calculated value on the sample of length $L$ and $F(L_c)$ the flux value calculated on the same sample after high-pass filtering at the cutoff wavelength $L_c$. *Mann and Lenschow* [1994] obtained the following parameterization of $\varepsilon_s$ from aircraft data gathered in the convective boundary layer

$$\varepsilon_s = bZ_i (z / Z_i)^{1/2} (L_c^{-1} - L^{-1}) \tag{7}$$

where $b$ is a coefficient (Mann and Lenschow proposed $b$=1.2), $Z_i$ is the boundary layer thickness, and $z$ the altitude of the sample. We can note that $\varepsilon_s$ in (6) can be either positive or

negative, which results from the fact that the filtered flux can be lower than or greater than the nonfiltered flux, respectively. On the contrary, $\varepsilon_s$ as expressed by (7) is positive (because $L_c<L$), which results from the fact that the filtered flux is, on average (for the data under consideration), lower than the nonfiltered flux. Furthermore, $\varepsilon_s$ does not depend on the flux; that is, it has the same value for, for example, the sensible heat flux, latent heat flux, and momentum flux. We can obtain a direct estimation of the systematic error from the difference between the nonfiltered flux and the high-pass filtered flux. This difference can be computed for different cutoff frequencies. The results can thus be compared to the parameterization proposed in (7).

The random error $\varepsilon_a$ is defined for a Gaussian process as [*Wyngaard*, 1983]

$$\varepsilon_a = (\sigma_{F(L)})/|F| = [2l_F L^{-1}(1 + r_F^{-2})]^{1/2} \quad (8)$$

where $l_F$ is the integral scale of the instantaneous flux (for instance, the integral scale of the $w'\theta'$ signal for the sensible heat flux) and $r_F$ is the correlation coefficient between the two signals involved in the definition of the flux. This error expresses the scatter we should obtain from series of realizations of the flux for a sample of length $L$. Parameterizations of the integral scales and of the random errors in the convective ABL have been proposed by *Lenschow and Stankov* [1986]. However, we can consider that we have two independent realizations of the same random process for the fluxes calculated along a run from the two aircraft. So the difference between the two aircraft is a direct estimation of the random error. We shall therefore be able to compare the standard deviation of this difference with the theoretical estimations provided by (8).

### 5.2. Results

Direct estimation of the error has been made for signals high-pass filtered with four cutoff wavelengths: 250, 1000, 2500, and 5000 m. Calculations have also been made for nonfiltered signals. The latter will be represented on the following graphs by points corresponding to a cutoff of 25 km, which is about the length of the samples. To estimate $\varepsilon_s$ from (7), the ABL thickness $Z_i$ was estimated from the thermodynamic and turbulence profiles. It was found at 1800 m. However, the systematic error for $L_c$=25 km was calculated with $L=\infty$. This corresponds to the error that would have been made with a 25 km filtering on a sample of infinite length. The other values were calculated with $L$=25 km, which approximately corresponds to the samples length. The principal problem for random error calculation with (8) is to calculate the integral scale $l_F$. It was deduced from the autocorrelation function of the instantaneous flux $w'X'$. In practice, it corresponds to the first zero of this function. To summarize, systematic error can be determined either directly from the difference between nonfiltered and filtered flux or from parameterization (7); random error can be determined either directly from the rms of the flux difference between the two aircraft or from the theoretical expression (8). Hereafter we will call them "direct" errors and "parameterized" errors.

Figure 13 shows these errors directly calculated and deduced from (7) and (8). The results were averaged at two flight levels and relate to $w'\theta'$ (which is proportional to the sensible heat flux), $w'q'$ (which is proportional to the latent heat flux), and $w'u'$ (which is proportional to the longitudinal component of the momentum flux). We shall first discuss the parameterized errors (Figures 13a and 13c). The systematic error decreases when the cutoff wavelength increases. However, the random error for the heat fluxes slightly increases when the cutoff wavelength increases. We can translate that as filtering being a compromise between these two errors. We can see that the 5 km cutoff wavelength represents a good compromise between the two errors because they are of about the same amount. In the past, an unwritten rule was often invoked to choose the cutoff of the filter at a wavelenth corresponding to 10 times the thickness of the boundary layer. For this case, $Z_i$ = 1800 m, and this rule has not therefore been followed. However, the average thickness of the mixed layer for a lot of experiments during SEMAPHORE analyzed by *Lambert and Durand* [1998] is about 900 m. Furthermore, increasing the cutoff wavelength would result in a considerable increase in random error on the flux estimation (see Figure 13).

Random error is generally greater for sensible heat flux than for latent heat flux. This can be explained by the low level of sensible heat flux. However, the parameterization of the random error for $u'w'$ presents very high values, always greater than 100%, which seems meaningless. Lastly, we can see that both errors are greater at 300 m than at 90 m, which is related to the increase in the turbulent characteristic scales with the altitude in the ABL.

From the direct estimations of the errors (Figures 13b and 13d), we can deduce the following conclusions. As for the results obtained from (7) and (8), direct estimations of the systematic and random errors are greater at 300 m than those obtained at 90 m. Moreover, systematic errors decrease when the cutoff wavelength increases. Unlike (7), we can see that the direct systematic error for the sensible heat flux is greater than that for the latent heat flux. The systematic error on $\overline{u'w'}$ is close to that obtained for the latent heat.

If we now consider the direct random error, it increases as expected at 90 m with the cutoff wavelength for sensible and latent heat fluxes but does not act the same way for momentum flux, with a minimum at a cutoff of 2500 m. At 300 m, the errors are greater than at 90 m for the three fluxes. The evolution of the errors according to the wavelength cutoff is not well marked.

If we compare parameterized and direct errors, we obtain almost the same values, but there are some differences; for heat fluxes, direct estimations are greater than parameterizations, especially for the sensible heat flux at 300 m. Nevertheless, this flux is weak at this altitude (about 5 to 10 W m$^{-2}$), which explains the increase in the errors. For the momentum flux random errors, we can see that direct estimations are more reasonable than parameterized ones, the latter appearing meaningless.

Finally, we can conclude from this work that the expected accuracy of the flux computations ranges from 10 to 20% at 90 m and from 20 to 60% at 300 m for sensible and latent heat flux. For momentum flux, the accuracy is about 30% at 90 m and about 100% at 300 m.

## 6. Conclusions

Aircraft-to-aircraft intercomparison is indispensable before analyzing the set of data obtained from cooperative experiments involving several aircraft. The two aircraft used for in situ measurements during SEMAPHORE generally

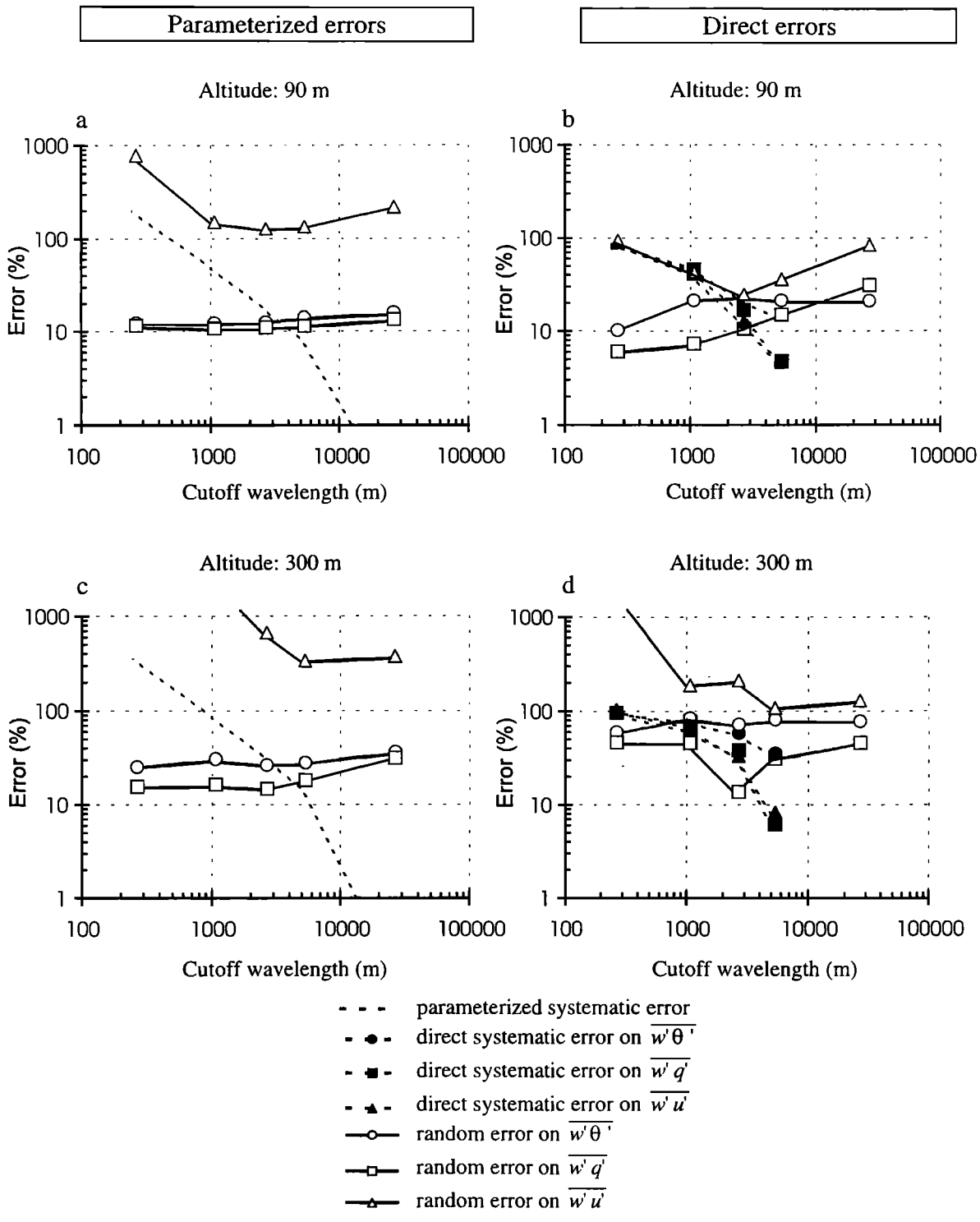


**Figure 13.** (Figures 13a and 13c) Parameterized and (Figures 13b and 13d) direct errors as a function of the cutoff wavelength. Results from the runs performed at (Figures 13a and 13b) 90 m and (Figures 13c and 13d) 300 m.

agree well; the mean parameters (thermodynamics and wind) concord well, except the temperature, which has to be adjusted between the two aircraft. It has to be noted that there is no absolute "external" reference for aircraft measurements and that we only can obtain a coherence between the two aircraft. The absolute accuracy of mean thermodynamic measurements cannot be known. This must be taken into account when using aircraft measurement for bulk parameterization of turbulence fluxes, for example.

Turbulence moments generally agree well, except for the momentum flux, which presents considerable scatter. The scatter is lower for variances than for fluxes and skewness, as expected. A thorough analysis of systematic and random errors on flux computations, following the work of *Lenschow*

*and Stankov* [1986] and of *Mann and Lenschow* [1994], revealed that the high-pass filtering of the signals at a cutoff wavelength of 5 km is a satisfactory compromise to minimize the total error in flux computation. The best accuracy is obtained for latent heat flux whose computation shows errors lower than those of sensible heat flux, which can be explained by the weakness of the latter. Momentum flux presents the poorest accuracy, probably because of the weakness of friction on the sea and of the great values of the integral scales for momentum transfer. However, direct estimations of the random error on momentum flux are considerably lower than those deduced from theoretical estimations. As a consequence, momentum flux can be determined from low-altitude airborne measurements with reasonable accuracy.

**Acknowledgments.** Many people were involved in the realization of the aircraft missions of SEMAPHORE and in the data processing. Among others, we would like to express our gratitude to L. Eymard, who manages the SEMAPHORE program; to J.C. Morin and G. Mariet for their help in the practical organization; to B. Bénech, J.L. Brenguier, A. Druilhet, and A. Weill, who contributed to the airborne campaign; to S. Prieur for his contribution to the data processing during the experiment; to people from the Division Technique de l'INSU, the Centre d'Aviation Météorologique, the team Mesures Météorologiques Aéroportées and to Bertrand Ferret, who processed the data; to the crews of the two aircraft, from the Institut Géographique National and from the Centre d'Aviation Météorologique, who tried to satisfy the wishes of the scientists; and to F. Saïd for fruitful discussions. This work was financially supported by the Programme Atmosphère Météorologique et Océan à Moyenne Echelle of INSU/CNRS.

## References

Brown, E. N., C. A. Friehe, and D. H. Lenschow, The use of pressure fluctuations on the nose of an aircraft for measuring air motion, *J. Clim. Appl. Meteorol., 22*, 171-180, 1983.

Dobosy, R. J., T. L. Crawford, J. I. MacPherson, R. L. Desjardins, R. D. Kelly, S. P. Oncley, and D. H. Lenschow, Intercomparison among four flux aircraft at BOREAS in 1994, *J. Geophys. Res., 102*, 29,101-29,111, 1997.

Druilhet, A., and P. Durand, Experimental investigation of atmospheric boundary layer turbulence, *Atmos. Res., 43*, 345-388, 1997.

Druilhet, A, D. Guédalia, J. Noilhan, and C. Charpentier, Moyens aéroportés utilisés durant l'expérience COCAGNE, *J. Rech. Atmos., 19*, 369-398, 1985.

Durand, P., H. Dupuis, D. Lambert, B. Bénech, A. Druilhet, K. Katsaros, P. K. Taylor, and A. Weill, Comparison of sea surface flux measured by instrumented aircraft and ship during SOFIA and SEMAPHORE experiments, *J. Geophys. Res.*, this issue.

Eymard, L. et al., Study of the air-sea interactions at the mesoscale: The SEMAPHORE experiment, *Ann. Geophys., 14*, 986-1015, 1996.

Kaimal, J. C., J. C. Wyngaard, D. A. Haugen, O. R. Coté, Y. Izumi, S. J. Caughey, and C. J. Readings, Turbulence structure in the convective boundary layer, *J. Atmos. Sci., 33*, 2152-2168, 1976.

Lambert, D., and P. Durand, The marine atmospheric boundary layer during SEMAPHORE. I: Mean vertical structure and non-isotropy of turbulence, *Q. J. R. Meteorol. Soc.*, in press, 1998.

Lenschow, D. H., Aircraft measurements in the boundary layer, in *Probing the Atmospheric Boundary Layer*, edited by D. H. Lenschow , pp. 39-56, Am. Meteorol. Soc., Boston, Mass, 1986.

Lenschow, D. H., and B. B. Stankov, Length scales in the convective boundary layer, *J. Atmos. Sci., 43*, 1198-1209, 1986.

Lenschow, D. H., and L. Kristensen, Applications of dual aircraft formation flights, *J. Atmos. Oceanic Technol., 5*, 715-726, 1988.

Lenschow, D. H., E. R. Miller, and R. B. Friesen, A three-aircraft intercomparison of two types of air motion measurement systems, *J. Atmos. Oceanic Technol., 8*, 41-50, 1991.

Lucotte, M., and F. Saïd, Comparaison des mesures de flux de surface obtenues par avion ou par stations sol au cours de l'expérience HAPEX Sahel, in *Proceedings of the "Atelier Expérimentation et Instrumentation,"* 6 pp., Météo-France, Toulouse, France, 1996.

Mann, J., and D. H. Lenschow, Errors in airborne flux measurements, *J. Geophys. Res., 99*, 14,519-14,526, 1994.

Nicholls, S., W. Shaw, and T. Hauf, An intercomparison of aircraft turbulence measurements made during JASIN, *J. Clim. Appl. Meteorol., 22*, 1637-1648, 1983.

Quante, M., P. R. A. Brown, R. Baumann, B. Guillemet, and P. Hignett, Three-aircraft intercomparison of dynamical and thermodynamical measurements during the Pre-Eucrex campaign, *Contrib. Atmos. Phys., 69*, 129-146, 1996.

Shaw, W. J., and J. A. Businger, Intermittency and the organization of turbulence in the near-neutral marine atmospheric boundary layer, *J. Atmos. Sci., 28*, 918-928, 1985.

Strom, J., R. Busen, M. Quante, B. Guillemet, P. R. A. Brown, and J. Heintzenberg, Pre-EUCREX intercomparison of airborne humidity measuring instruments, *J. Atmos. Oceanic Technol., 11*, 1392-1399, 1994.

Webb, E. K., G. I. Pearman, and R. Leuning, Correction of flux measurements for density effects due to heat and water vapour transfer, *Q. J. R. Meteorol. Soc., 196*, 85-100, 1980.

Wyngaard, J. C., Lectures on the planetary boundary layer, in *Mesoscale Meteorology-Theories, Observations and Models*, edited by D. K. Lilly and T. Gal-Chen, pp. 603-650, D. Reidel, Norwell, Mass., 1983.

P. Durand, Centre National de Recherches Météorologiques / Groupe de Météorologie Expérimentale et Instrumentale, 42 avenue Coriolis, 31057 Toulouse, France. (e-mail: Pierre.Durand@meteo.fr)

D. Lambert, Laboratoire d'Aérologie Observatoire Midi-Pyrénées, 14 avenue E. Belin 31400 Toulouse, France. (e-mail: lamd@aero.obs-mip.fr)

(Received December 31, 1996; revised June 27, 1997; accepted July 30, 1997.)